Mechanism of the Hydrazine Hydrate Electrooxidation Reaction on Metallic Ni Electrodes in Alkaline Media as Revealed by Electrochemical Methods, Online DEMS and Ex situ XPS

Evgeniia Vorms, Vasiliki Papaefthymiou, Théo Faverge, Antoine Bonnefont, Marian Chatenet, Elena Savinova, Alexandr Oshchepkov

Mechanism of the Hydrazine Hydrate Electrooxidation Reaction on Metallic Ni Electrodes in Alkaline Media as Revealed by Electrochemical Methods, Online DEMS and Ex situ XPS

Evgeniia A. Vorms,[a] Vasiliki Papaefthymiou,[a] Théo Faverge,[b] Antoine Bonnefont,[b] Marian Chatenet,[b] Elena R. Savinova[a], Alexandr G. Oshchepkov [a,]*

[a] Institut de Chimie et Procedés pour l'Energie, l'Environnement et la Santé, UMR 7515 CNRS – University of Strasbourg, 67087 Strasbourg Cedex, France

[b] University Grenoble Alpes, University Savoie Mont Blanc, CNRS, Grenoble INP (Institute of Engineering, University Grenoble Alpes), LEPMI, 3800 Grenoble, France

* Corresponding Author, E-mail: aoshchepkov@unistra.fr

KEYWORDS

Nickel; Hydrazine hydrate electrooxidation reaction (HHOR) mechanism; Alkaline media; Nickel hydroxide; Surface poisoning

HIGHLIGHTS

- Metallic Ni catalyzes the HHOR below the reversible hydrogen electrode potential.
- Ni catalyzes 4-electron HHOR, suggesting complete hydrazine oxidation.
- ~~H_{ads} is the HHOR intermediate on Ni.~~
- OH^- and OH_{ads} are the reactive species for the HHOR on Ni.
- Strongly adsorbed NH_x species formed during the HHOR partially block Ni surface.

ABSTRACT

Metallic Ni surface was examined as a catalyst for the hydrazine hydrate oxidation reaction (HHOR) by cyclic voltammetry, chronoamperometry, and *on-line* differential electrochemical mass-spectrometry (DEMS). It was found that N_2 is a sole gaseous product formed during the HHOR on Ni and 4 electrons are transferred in the process, which corresponds to a complete oxidation of the hydrazine molecule. The mechanism of the HHOR on the Ni surface involves OH^- and adsorbed OH_{ads} intermediate, the latter improving the rate of the HHOR. Ni catalysts were found to be poisoned during the HHOR, the extent of poisoning depending on the number of surface sites, hydrazine concentration, and the α-$Ni(OH)_2$ coverage. *Ex situ* X-ray photoelectron spectroscopy (XPS) measurements were performed to characterize the species poisoning Ni surface.

1 INTRODUCTION

Society faces major challenges of resource depletion, environmental pollution and greenhouse effect, as a result of continuous growth of the fossil fuel (oil, natural gas and coal) consumption, the latter producing gigantic amounts of CO_2. Electrochemical energy production from carbon-free fuels has recently attracted significant attention. Nowadays the most technologically-advanced fuel cells (FCs) are proton-exchange membrane fuel cells (PEMFCs) running on hydrogen. However, using hydrogen as a fuel causes safety issues, since it is stored under high pressure in heavy tanks, the weight of the tank also reducing the overall specific energy of the stored fuel. Moreover, PEMFCs operate in acidic media, narrowing the number of metals that can be used as catalysts for hydrogen oxidation (HOR) and oxygen reduction (ORR) reactions down to (almost) only Pt-based catalysts [1]. Direct liquid fuel cells (DLFCs) that run on liquid fuel are considered promising alternatives to PEMFCs, for example, for portable and mobile applications. Such a concept simplifies fuel storage and transportation and allows the use of non-noble metal catalysts since fuels in DLFCs are typically dissolved in alkaline solutions. Hydrazine is one of the most promising fuels because the hydrazine hydrate oxidation reaction (HHOR, forward step of eq. 1) has a low standard potential compared to the HOR (forward step of eq. 2). Furthermore, full HHOR leads to production of environmentally-friendly N_2 and H_2O, and transfer of 4 electrons, while only 2 are produced during the HOR:

$$N_2H_4 + 4OH^- \rightleftarrows N_2 + 4H_2O + 4e^- \qquad (E^0 = -0.32 \text{ V vs. RHE, eq. 1})$$

$$H_2 + 2OH^- \rightleftarrows H_2O + 2e^- \qquad (E^0 = 0 \text{ V vs. RHE, eq. 2})$$

However, the number of electrons transferred in the HHOR can be reduced due to the occurrence of side hydrazine decomposition reactions (eqs. 3, 4):

$3N_2H_4 \rightarrow 4NH_3 + N_2$ (eq. 3)

$N_2H_4 \rightarrow N_2 + 2H_2$ (eq. 4)

Ni is recognized as a good catalyst for the HHOR, notably due to its low cost and stability in alkaline media. However, to the best of the authors' knowledge, until now the products of the HHOR on Ni have not been studied. Furthermore, published data regarding the catalytic activity of Ni in the HHOR are contradictory, some studies reporting HHOR at potentials close to [2–5] or even below [6–9] 0 V vs. RHE, the other reporting very high HHOR "onset"[1] potentials (E > 0.6 V vs. RHE) [10–12]. The presence of a second element in the catalyst composition [3,7,9–16] further complicates the analysis, due to its possible involvement in the HHOR, as was shown, for example, for Co [17]. Besides, the second element can affect the Ni surface state, thus indirectly affecting its reactivity [18]. Indeed, Jeon et al. [5] found that after heat-treatment in the hydrogen atmosphere (at 400°C for 4 h under a flow of 5 vol.% H_2 and 95 vol.% N_2), the Ni activity in the HHOR increases along with the metallic Ni^0 fraction on the surface, thus pointing to the importance of the Ni surface state for the HHOR. It was also suggested that high coverages of surface α-$Ni(OH)_2$ cause a decrease of the Ni activity in the HHOR [17]; however, the α-$Ni(OH)_2$ coverage influence on the HHOR mechanism

[1] Albeit the term "onset potential" is often misused in the literature, here and in what follows is used for simplicity to semi-quantify the potential at which currents become experimentally observable. It should be noted however that along with the hydrazine oxidation other anodic and cathodic (e.g. hydrogen evolution reaction, HER) processes may contribute to the measured current.

has not been studied in detail yet. Besides, it is widely accepted that hydrazine does not involve any poisoning effect, due to the absence of the carbon atom in the structure and therefore inability to produce poisoning species such as CO or C_2-molecules [19–22]. However, those are not the only species that can poison the catalyst surface; the fact that poisoning of the Ni surface during the HHOR has never been explored systematically is a clear lack in the literature.

In this study, to fill the gaps in the current understanding of the HHOR mentioned above, Ni catalysts are investigated for the HHOR in low potential window, paying special attention to keep its surface in the metallic state. For the first time, products of the HHOR on metallic Ni are determined by differential electrochemical mass-spectrometry (DEMS). Cyclic voltammetry/chronoamperometry experiments are performed up to/at different potentials to shed light on the role of Ni-OH_{ads} and α-$Ni(OH)_2$ in the HHOR. Finally, the presence of adsorbates poisoning the Ni surface during the HHOR is evaluated with the help of *ex situ* X-ray photoelectron spectroscopy (XPS), taking into account the effect of α-$Ni(OH)_2$ formation on this process.

2 EXPERIMENTAL

2.1 Materials

$NiSO_4 \cdot 6H_2O$ (99.99% Aldrich), $(NH_4)_2SO_4$ (99,95%, Aldrich), N_2H_4 (64-65 wt.%, 99%, Sigma-Aldrich), HNO_3 (67-69%, Fisher Chemical), and NaOH (50 wt.% in water, Aldrich) were used as received. For electrochemical experiments, all solutions were prepared using purified water (18.2 MΩ cm, TOC < 2 ppb) and purged with high-purity gases (N_2 99.99%, Ar 99.999%). Prior to each

experiment, the Teflon- and glassware was cleaned by soaking in a H_2SO_4:H_2O_2 (1:1 v/v) mixture and then thoroughly washed with ultrapure water.

2.2 Preparation of Ni electrodes

2.2.1 Ni nanoparticles on carbon

To prepare carbon suspension, 3.25 mL of isopropanol was added to 5 mg of Vulcan XC-72R (Cabot) carbon black, followed by ultrasonication of the mixture in the ice-cooled water bath for 15 min. Then, 1.75 mL of purified water was added to the suspension and the mixture was again ultrasonicated in the ice-cooled water bath for an additional 15 min. A glassy carbon (GC) disk (Ø 5 mm, geometric surface area S_{geom} = 0.196 cm^2, Sigradur G) was polished with Al_2O_3 powder (0.3 µm) for 5 minutes, then ultrasonicated in ethanol, acetone and purified water (5 min in each solvent). After that 4 µL of the carbon suspension was applied on the surface of the GC disk and dried under N_2 flow for 3 min, the procedure was repeated 5 times to attain carbon loading of ~ 100 µg cm^{-2} on the GC disk (C/GC). Ni nanoparticles (Ni/C) were electrodeposited on C/GC at room temperature (22 ± 2°C) from aqueous solutions of 0.1 M $(NH_4)_2SO_4$ + 0.01 M $NiSO_4$ with pH equal to 4.4 under the rotation rate of 400 rpm in a three-electrode glass cell with the three compartments for counter electrode (Au wire), working electrode (C/GC) and reference electrode (mercury-mercurous sulfate electrode, MSE, E_{MSE} = 0.96 V vs. RHE) by applying E = -1.45 V vs. MSE until charge of 150 mC was reached.

2.2.2 Polycrystalline Ni rod

Ni rod (polycrystalline Ni) was polished with Al_2O_3 powder (0.3 μm) for 15 minutes, then ultrasonicated in water for 30 s and quickly (< 20 s) transferred to the electrochemical cell with a drop of water to minimize oxidation of the Ni surface by oxygen from air.

2.3 Electrochemical measurements

Electrochemical measurements were carried out in a three-electrode Teflon cell at room temperature (22 ± 2°C) with the gold wire as a counter electrode and Hg/HgO/1 M NaOH as a reference electrode ($E_{Hg/HgO}$ = 0.93 V vs. RHE). Cyclic voltammograms (CVs) were recorded for Ni catalysts (Ni/C and polycrystalline Ni) in 1 M NaOH purged with N_2 in the potential intervals from -0.2 to 0.4 V vs. RHE (3 scans), and from -0.06 to 0.4 V vs. RHE (3 scans) at the scan rate (v) of 20 mV s^{-1}. The latter CVs were used for the estimation of the electrochemically active surface area (ECSA) of Ni, determined from the anodic charge and the conversion coefficient (0.514 mC cm^{-2}) [23]. Then the electrode was cycled between -0.2 and 0.4 V vs. RHE (3 scans) at v = 20 mV s^{-1} to ensure the metallic state of Ni surface before testing its activity in the HHOR. For the HHOR measurements, a calculated volume of 5 M N_2H_4 + 1 M NaOH solution was added directly into the Teflon cell to obtain the desired N_2H_4 concentration.

For the chronoamperometry measurements in N_2-purged 1 M NaOH + 5 mM N_2H_4 electrolyte, -0.25, -0.20, -0.15, -0.10, -0.05, 0, 0.05, 0.10, 0.15, 0.20 and 0.25 V vs. RHE potentials were sequentially applied, each for 5 min, and the electrode was rotated at a speed (ω) of 1600 rpm.

To perform the XPS measurements, a polycrystalline Ni disk was carefully washed with water and fixed on the sample holder immediately after the electrochemical treatment with a drop of purified

water on its top surface (aiming to minimize contact with the ambient atmosphere). After that, the sample was quickly (within 5 min) placed into the entry chamber of the XP spectrometer, degassed down to P ≈ 10^{-5} Pa, and then transferred to the main chamber of the XP spectrometer.

2.4 Materials characterization

The morphology of Ni/C samples was studied by transmission electron microscopy (TEM) using JEOL 2100F microscope operating at accelerating voltage of 200 kV.

The XPS measurements were performed in VSW Scientific spectrometer equipped with a hemispherical electron analyzer. The Al Kα *h*v = 1486.6 eV monochromatic X-ray source was used as incident radiation. The constant pass energy mode was used to record both survey and high-resolution spectra, with pass energies of 90 and 44 eV respectively. The charging effect arising in the process of photoemission of electrons was considered by correcting the spectra with respect to C1s of the carbon line set at 284.6 eV. XP spectra were curve-fitted after Shirley background subtraction, following the procedure described in Ref. [24].

2.5 *On-line* DEMS measurements

On-line DEMS measurements were carried out with a Pfeiffer Vacuum QMA 200 quadrupole mass spectrometer using two differentially pumping chambers. A three-electrode glass cell was used for the simultaneous electrochemical measurements with a Ni electrode, a Au wire and the RHE as the working, counter, and reference electrodes, respectively. The Ni electrode was prepared by electrodeposition of Ni particles on top of the PTFE membrane pre-covered with a thin layer of sputtered Ni (Ni/Ni_{spt}, S_{geom} = 1.13 cm^2). The deposition was performed from 0.1 M $(NH_4)_2SO_4$ + 0.01

M $NiSO_4$ solution at -1.45 V vs. MSE by passing 8 mC charge. The hydrazine electrooxidation products were monitored at mass/charge ratios of m/z = 28 (N_2), 2 (H_2), 17 (NH_3), 30 (NO), 46 (NO_2), and 44 (N_2O). During the measurements, the 1 M NaOH + 5 mM N_2H_4 electrolyte was purged with Ar to deoxygenate the solution and ensure its agitation.

3 RESULTS AND DISCUSSION

3.1. Ni activity in the HHOR

TEM analysis of Ni/C samples (Fig. 1) revealed a wide particle size distribution from 10 to 50 nm with the highest fraction of particles in the size interval from 20 to 30 nm (Fig. 1d). In addition, TEM images at high resolution clearly indicate that 20 – 50 nm Ni particles comprise of smaller interconnected crystallites (see e.g. Fig. 1c). The particles are therefore essentially polycrystalline.

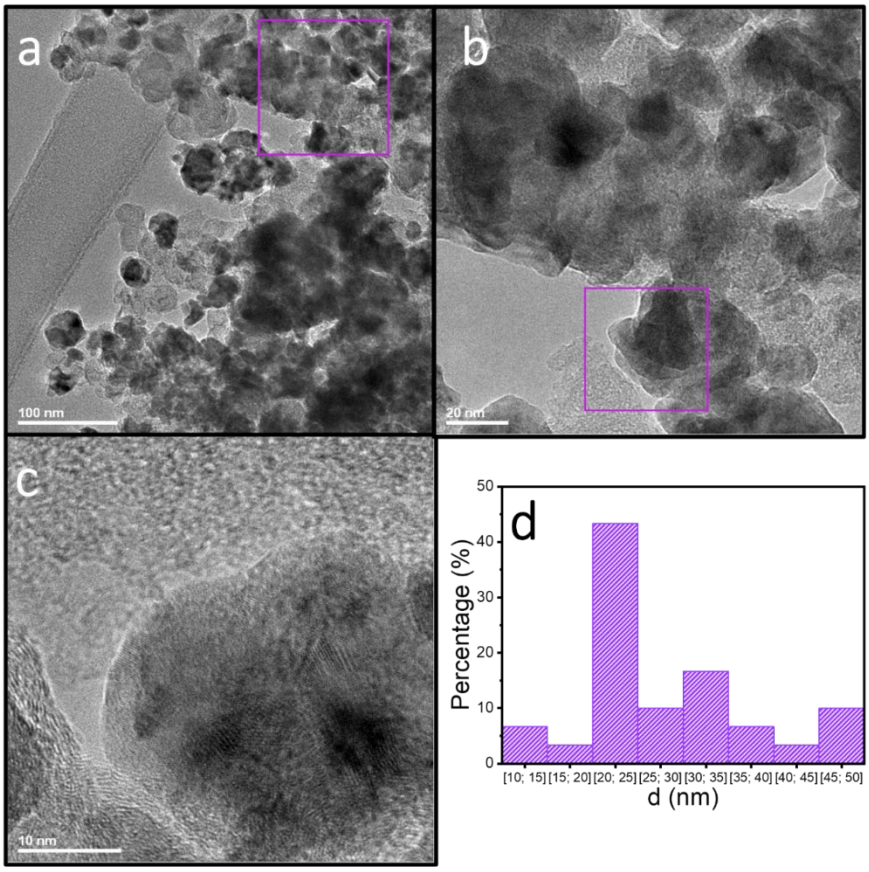

Fig. 1. (a, b) Low- and (c) high-resolution TEM images of a Ni/C sample and (d) the Ni particles size distribution.

Fig. 2a shows typical CVs recorded for metallic Ni/C in alkaline media, demonstrating characteristic features of metallic Ni with well-defined anodic (between 0 and 0.4 V vs. RHE) and cathodic (between -0.15 and 0.2 V vs. RHE) peaks. The shape of CV being very sensitive to the surface state, special efforts have been made in this work to keep Ni in its metallic state (by minimizing contact of samples with the atmosphere, and avoiding application of potentials above 0.4 V vs. RHE). Based on the microkinetic modeling, it has been suggested [24–26] that several electrochemical

steps contribute to the peaks observed on the CV curves, namely H adsorption/desorption (eq. 5), OH adsorption/desorption (eq. 6), and formation of a monolayer of α-$Ni(OH)_2$ (eq. 7).

$$H_{ads} + OH^- \rightleftarrows H_2O + \bar{e} \quad \text{(eq. 5)}$$

$$Ni + OH^- \rightleftarrows Ni\text{-}OH_{ads} + \bar{e} \quad \text{(eq. 6)}$$

$$Ni\text{-}OH_{ads} + OH^- \rightleftarrows Ni(OH)_2 + \bar{e} \quad \text{(eq. 7)}$$

On the anodic scan (Fig. 2b) $Ni\text{-}OH_{ads}$ formation (eq. 6) occurs above 0 V vs. RHE after electrochemical desorption of hydrogen (eq. 5), which is strongly adsorbed on metallic Ni [24,27]. At E > 0.1 V vs. RHE, formation of α-$Ni(OH)_2$ proceeds (eq. 7), the latter being fully reduced on the cathodic scan (at least if the anodic potential limit is kept below 0.5 V vs. RHE [28]). As one may notice, in the case of cycling Ni/C between -0.25 and 0.3 V vs. RHE (Fig. 2a), the Ni surface is not fully covered with α-$Ni(OH)_2$, which leads to the smaller cathodic peak on the backward (cathodic) scan.

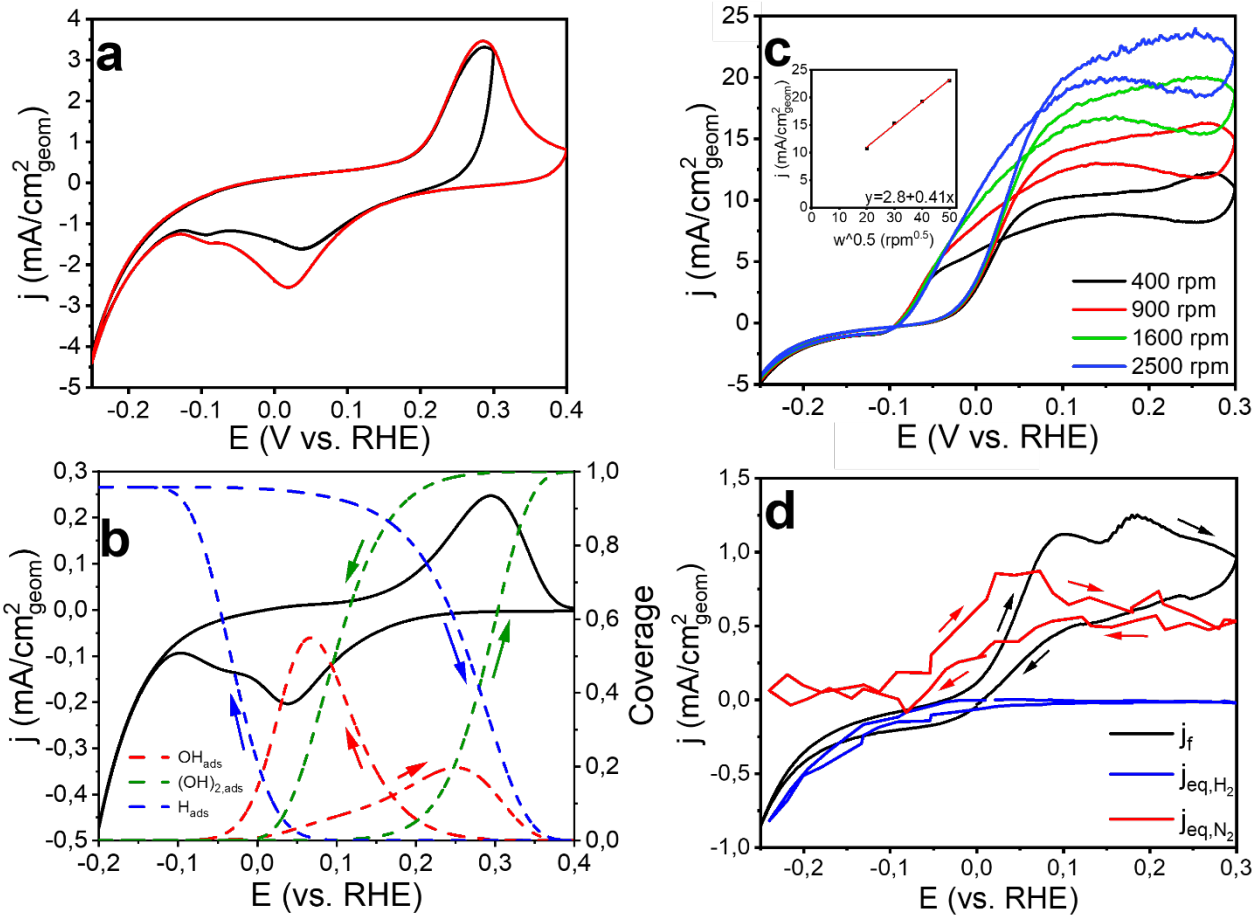

Fig. 2. (a, c) Cyclic voltammograms for a Ni/C sample in N_2-saturated (a) 1 M NaOH at v = 20 mV s^{-1} and (c) 1 M NaOH + 5 mM N_2H_4 at v = 20 mV s^{-1} and different rotation rates indicated on the plot. The inset in panel (c) shows Levich plot at 0.2 V vs. RHE for the anodic scan; (b) Simulated cyclic voltammogram (solid curve) and the coverage (dashed curves) of the electrode surface by various adsorbates for metallic polycrystalline Ni in 0.1 M NaOH at v = 20 mV s^{-1}. The curves are plotted using the parameters taken from Ref. [25]; (d) DEMS measurements for a Ni/Ni_{spt} sample in Ar-saturated 1 M NaOH + 5 mM N_2H_4 at v = 20 mV s^{-1}. Ionic currents (H_2 and N_2) are recalculated into the faradaic ones ($I_{eq,H2}$, and $I_{eq,N2}$) using the calibration constants (K_{H2} = 2.2*10^{10}, K_{N2} = 1.8*10^{11}) determined from the HER potential interval for H_2 and the HHOR taking place from -0.05 to 0.1 V vs. RHE for N_2.

The RDE CVs recorded in 5 mM N_2H_4 solution for Ni/C (Fig. 2c) show that the HHOR "onset" potential lies at E = -0.05 V vs. RHE, and diffusion-limited currents are reached at E > 0.10 V vs. RHE. The slight increase of the oxidation currents in the anodic scan at potentials between 0.2 and 0.3

V vs. RHE is due to the overlap of the HHOR currents and α-$Ni(OH)_2$ formation currents. The obtained RDE CVs were further analyzed using Levich equation (one may notice a non-zero intercept of the Levich plot, which may result from contribution of non-stationary currents):

$$j = 0.62\ n\ F\ D^{2/3}\ \omega^{1/2}\ \nu^{-1/6}\ C(N_2H_4) = B\ \omega^{1/2} \quad \text{(eq. 8)}$$

with n – number of transferred electrons, F = 96485 C mol^{-1} – Faraday constant, D = 1.39*10^{-5} $cm^2\ s^{-1}$ [29] – diffusion coefficient of N_2H_4, ω [rad s^{-1}] – rotation rate, ν [$cm^2\ s^{-1}$] – kinematic viscosity of 1 M NaOH, and $C(N_2H_4)$ = 5 mM – concentration of N_2H_4.

$$\nu = \eta/\rho \quad \text{(eq. 9)}$$

where η = 1.129 mPa s^{-1} and ρ = 1.039 g cm^{-3} are the dynamic viscosity and density of 1 M NaOH, respectively [30].

Based on the slope of Levich plot at 0.2 V vs. RHE, the number of transferred electrons during the HHOR was estimated to be close to 4, suggesting that the main process is the complete electrooxidation reaction of N_2H_4 with the formation of N_2 (eq. 1). This conclusion was confirmed by DEMS experiments (Fig. 2d), as no gaseous products except N_2 were detected at potentials where the HHOR currents are observed (Fig. S1). H_2 was detected at E < 0 V vs. RHE and is attributed to the hydrogen evolution reaction (HER). One can notice that N_2 formation starts below the HHOR "onset" potential on the Ni/Ni_{spt} electrode. This partially arises from the inclined CV shape (likely due to imperfect isolation of the connection between the sample and current collector) as well as oxygen traces in the electrochemical cell, resulting in reduction currents (see Fig. S2). However these experimental drawbacks cannot fully explain the apparent difference between I_f and $I_{eq,N2}$. Besides,

the $I_{eq,N2}$ signal in the interval from -0.1 to 0.1 V vs. RHE is higher on the anodic scan than on the cathodic one. Note also that NH_3, which could be formed as a product of the N-N bond breaking in N_2H_4, was not detected by DEMS. All of the above points at the occurrence of non-faradaic reactions in this potential interval, resulting in formation of adsorbates that can be oxidized only at E > -0.05 V vs. RHE. Based on the reasoning described above, one can assume that at on some Ni sites N-H bonds of N_2H_4 break already at E = -0.1 V vs. RHE, releasing N_2 and forming adsorbed hydrogen atoms (H_{ads}), as will be further discussed in Section 3.3.

Two waves are observed on the anodic scan of the CV recorded for Ni/Ni_{spt} (Fig. 2d): (i) between 0 and 0.15 V vs. RHE and (ii) between 0.15 and 0.3 V vs. RHE. Considering the DEMS results, and literature data evidencing that H_{ads} is oxidized on Ni at E > 0 V vs. RHE [25], the authors assume that the first oxidation wave is due to overlapping HHOR (eq. 1) and H_{ads} oxidation currents (eq. 5), while the second one can be explained by overlapping HHOR (eq. 1) and α-$Ni(OH)_2$ formation (eq. 7) currents. It should also be noted that the shape of CVs of Ni/Ni_{spt} in the DEMS setup is different from the one measured on Ni/C in the RDE configuration, with currents being much inferior to the diffusion-limited ones. This difference can be explained by a smaller ECSA of the Ni electrode used in DEMS experiments (*cf.* 10 times smaller than that of Ni/C), and absence of the electrode rotation in our DEMS setup (albeit some "stirring" was provided by permanently bubbling the solution with Ar).

To further access the role of various adsorbates in the HHOR, CVs of Ni/C in an N_2H_4 solution were measured in an RDE setup with variable anodic limit (Fig. 3a). One may notice that the cathodic scan is strongly affected by the anodic potential limit. Setting the anodic limit at 0.1 V vs. RHE,

currents on the anodic and cathodic scan are almost identical, while increasing it to 0.2 V vs. RHE results in "crossing" of the anodic and cathodic scans, HHOR currents in the potential interval between -0.1 and 0.05 V vs. RHE on the cathodic scan being significantly higher than on the anodic one. This observation implies that the HHOR is significantly improved in the presence of Ni-OH_{ads} species, the amount of which is expected to be larger on the cathodic scan according to the results of microkinetic modeling (Fig. 2b).

Chronoamperometry measurements were performed to access the temporal evolution of the HHOR currents (Figs. 3b, c). Notably, the crossing of the anodic and cathodic currents is absent in the chronoamperometry mode, independent on the point taken on the timeline (Fig. 3b). This indicates the similarity in the state of Ni surface on the anodic and cathodic plots under steady-state conditions, likely due to the absence of accumulated OH_{ads}/$(OH)_{2,ads}$ species in potentiostatic mode, these species being present on the surface under dynamic conditions. The observed difference further strengthens the hypothesis about the need of OH_{ads}-species for the HHOR current enhancement on Ni.

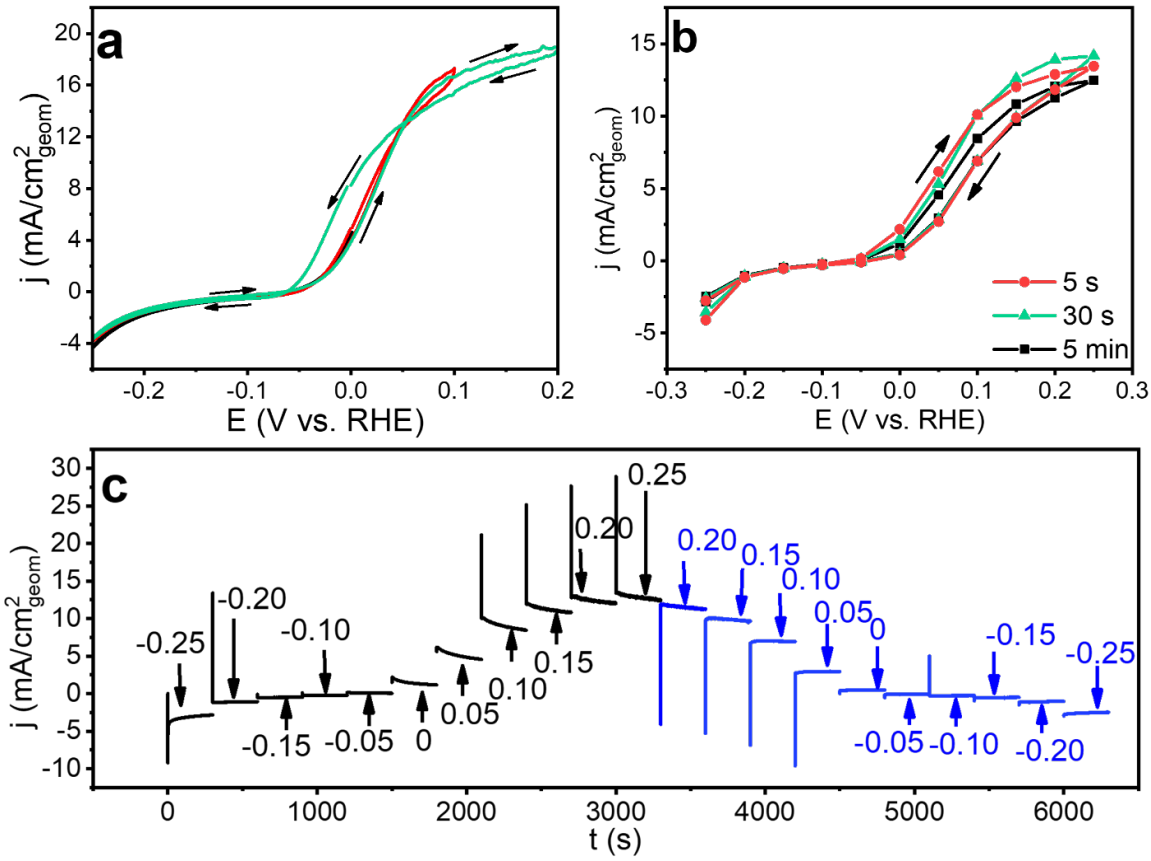

Fig. 3. (a) Cyclic voltammograms for a Ni/C sample in N_2-saturated 1 M NaOH + 5 mM N_2H_4 at v = 20 mV s^1 and ω = 1600 rpm with different anodic limits equal to 0, 0.1, 0.2 V vs. RHE; (b) Current-potential curves for Ni/C plotted at different times from (c) chronoamperometry measurements in N_2-saturated 1 M NaOH + 5 mM N_2H_4 at ω = 1600 rpm with 50 mV step and 5 min total polarization time.

3.2. Poisoning of metallic Ni by hydrazine

s

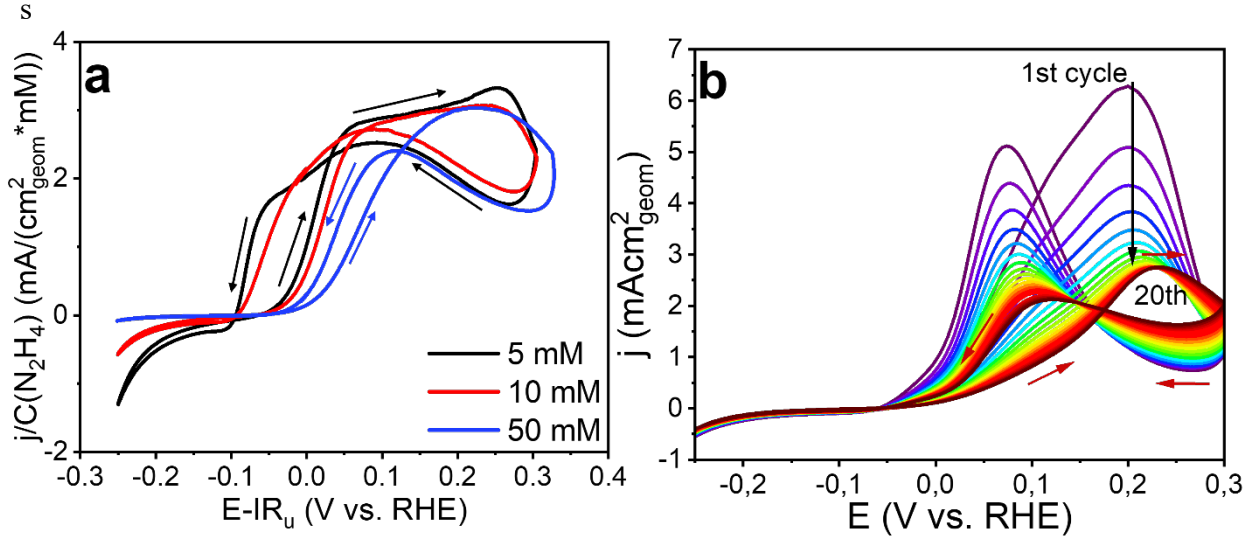

Fig. 4. Cyclic voltammograms at v = 20 mV s^{-1} and ω = 1600 rpm for (a) Ni/C in N_2-saturated 1 M NaOH + 5, 10, 50 mM N_2H_4 with currents normalized by the N_2H_4 concentration; (b) polycrystalline Ni in N_2-saturated 1 M NaOH + 5 mM N_2H_4.

Utilization of hydrazine as a fuel in fuel cell configuration requires stable anode and cathode operation. The objective of this section is to detect eventual Ni surface poisoning in the presence of hydrazine. To that goal, the influence of the hydrazine concentration on the performance of Ni/C electrodes is firstly explored. Fig. 4a shows CVs acquired for a Ni/C at different N_2H_4 concentrations (from 5 to 50 mM). To facilitate the analysis, currents are divided by the hydrazine concentration. One may see that an increase of the concentration leads to a decrease of the normalized oxidation currents at E < 0.05 V vs. RHE, both on the anodic and cathodic scans (Fig. 4a); this shifts the CVs to more positive potentials, implying formation of some strongly-adsorbed species that cover the Ni surface and inhibit its catalytic activity. In addition, the width of the hysteretic potential region decreases when the hydrazine concentration increases, confirming faster poisoning of the Ni surface during the cathodic scan in 50 mM hydrazine.

Secondly, the stability of the CVs to continuous potential cycling is analyzed. CVs for Ni/C in 5 mM N_2H_4 solution recorded in the interval from -0.25 to 0.3 V vs. RHE are relatively stable (Fig. S3). In the meantime, while recording 20 CVs for a polycrystalline Ni electrode (having 20 times less ECSA than Ni/C, Fig. S4) in the solution with N_2H_4 concentration of 5 mM, the "onset" potential shifts to positive potentials and HHOR currents are constantly decreasing (Fig. 4b). The latter indicates formation of adsorbates that progressively cover the surface of a polycrystalline Ni with a lower number of Ni sites compared to Ni/C. Analysis of the chronoamperometry measurements (Fig. 3c) further confirms this statement. Indeed, the current decay observed on the ascending curves is followed by the decrease of the HHOR currents on CVs registered right after applying a certain potential (Fig. S5). Besides, we note that the absolute currents measured at $E \leq -0.05$ V vs. RHE in the presence of hydrazine are slightly lower compared to the blank electrolyte (Fig. S6), which likely points to attenuation of the HER currents due to the surface blockage at low potential.

To shed more light on the surface poisoning and explore its dependence on the electrode potential, additional measurements were performed, consisting of the following steps: (i) firstly, CVs were recorded for metallic polycrystalline Ni in 1 M NaOH solution; (ii) then the circuit was open, and the OCP started to be recorded in 1 M NaOH; (iii) after that, a certain volume of concentrated $N_2H_4 \cdot H_2O$ was added directly into the cell to obtain a 5 mM N_2H_4 solution (this action causes a drop of the potential, as one may see in Fig. 5a), and the OCP was recorded for another 5 min; (iv) finally, the electrode was pulled out from the electrolyte containing N_2H_4 and put into the second cell with 1 M NaOH electrolyte (hydrazine-free), where CVs were recorded to electrochemically characterize the Ni surface (Fig. 5b). Fig. 5a shows two typical OCP transients: in

the first one (sample №1) the OCP reached before hydrazine injection was around 0.25 V vs. RHE (similar results were obtained at lower OCP), in the second case (sample №2) it was let to attain 0.37 V vs. RHE. Comparing OCP transients for samples №1 and №2, one may notice that the OCP for the sample №1 drops to 0 V vs. RHE after N_2H_4 addition, while OCP for the sample №2 drops slightly to reach 0.34 V vs. RHE, and then experiences further growth. This behavior is consistent with the assumption that hydrazine adsorption is very sensitive to the Ni surface state, and cannot proceed on the surface fully covered by α-$Ni(OH)_2$. Indeed, according to the previous modeling studies [24–26], at E > 0.3 V vs. RHE, the surface of Ni electrode is fully covered by α-$Ni(OH)_2$, while at E = 0.25 V vs. RHE, OH_{ads} is present on the surface along with α-$Ni(OH)_2$ (Fig. 2b). The fact that sample №1 experiences drop of the OCP to E ≈ -0.05 V vs. RHE, while sample №2 does not, strongly suggests that (adsorbed) hydrazine reacts with OH_{ads} species but not with α-$Ni(OH)_2$. Comparing CVs recorded for these two samples after the contact with the N_2H_4 solution (Fig. 5b), one can see that the α-$Ni(OH)_2$ formation peak is suppressed for the sample №1 but not for the sample №2 (CVs for both samples are stable) ~~suggesting the formation of poisonous species at negative potentials that block the Ni surface for OH_{ads} formation and therefore α-$Ni(OH)_2$.~~ This confirms that the poisoning species are not formed if the surface was initially almost fully covered with α-$Ni(OH)_2$. Moreover, this is in agreement with stronger adsorption of hydroxides compared to hydrazine at potentials above 0.3 V vs. RHE, leading to the drop of the HHOR current (Fig. S7).

Analysis of the experimental data suggests that surface poisoning is site-demanding, requiring several surface sites for hydrazine adsorption. Indeed, long cycling of polycrystalline Ni in 5 mM N_2H_4 solution leads first to a decrease of the HHOR current (Fig. 4b), followed by its stabilization or

even termination of the poisoning. However, if the surface is covered with α-$Ni(OH)_2$ or with poisoning species occupying a significant fraction of surface sites, the poisoning slows down or even stops. The latter explains the stabilization of the currents during chronoamperometry experiments (Fig. 3c) at E > 0.15 V vs. RHE on the forward scan, and absence of the HHOR and HER currents decrease at E < 0.1 V vs. RHE on the backward scan.

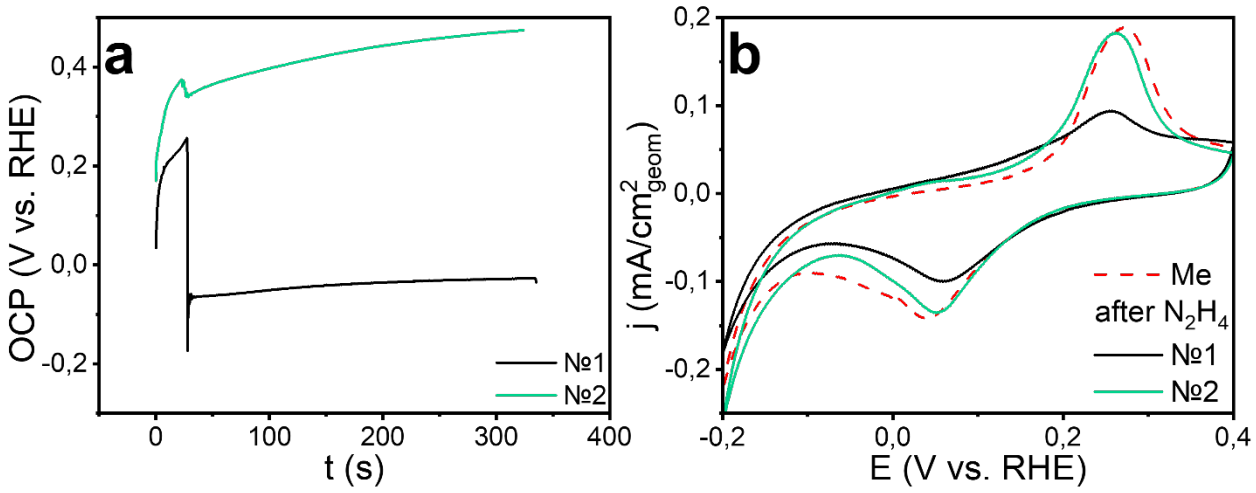

Fig. 5. (a) OCP recorded for polycrystalline Ni in 1 M NaOH + 5 mM N_2H_4, 1600 rpm, t = 5 min; (b) CVs recorded the polycrystalline Ni before and after contact with N_2H_4 solution in 1M NaOH at a scan rate (v) of 20 mV/s

To characterize the poisoning species, XPS measurements were made for polycrystalline Ni that was in contact with N_2H_4 for different time: 6 s (Figs. 6a, d), 40 s (Figs. 6b, e) and 100 s (Figs. 6c, f): increasing the time from 6 s to 40 s leads to an increase in the relative N/Ni atomic fraction from 0.04 to 0.20, the latter not experiencing further growth at longer time (Fig. S8). The data thus confirm the increase and then stabilization of the surface coverage by N-containing poisoning species with time. This increase of the N/Ni atomic fraction is accompanied by the decrease of the metallic Ni fraction in the analyzed samples, as shown in Figs. 6d-f. Two N1s peaks observed in Figs.

6a, b at low (400.0 ± 0.5 eV) and high (406.8 ± 0.2 eV) binding energy can be attributed to $N_2H_{x,ads}/NH_{x,ads}$ [31–34] and some oxidized nitrogen species NO_x species (e.g. nitrates), respectively [35]. The formation of nitrates can explain the decrease of the Ni^0 fraction; however, since the standard potential of nitrate formation from N_2H_4 (E^0 = 0.69 V vs. RHE) is much higher than the one established during the measurements (OCP < 0 V vs. RHE), it can be suggested that only $NH_{x,ads}$ and $N_2H_{x,ads}$ are present at the electrode surface exposed to hydrazine. These species may be further oxidized *ex situ* by oxygen from air during the transfer of the sample from the electrochemical cell to the XPS chamber. More precise analysis requires performing *in situ* XPS measurements, which are currently in progress and will be reported elsewhere. Finally, it is noted that N-containing species were absent in the controlled XPS measurements made for polycrystalline Ni held at -0.06 V vs. RHE (similar to OCP in Fig. 6) for 5 min in 1 M NaOH (Fig. S9).

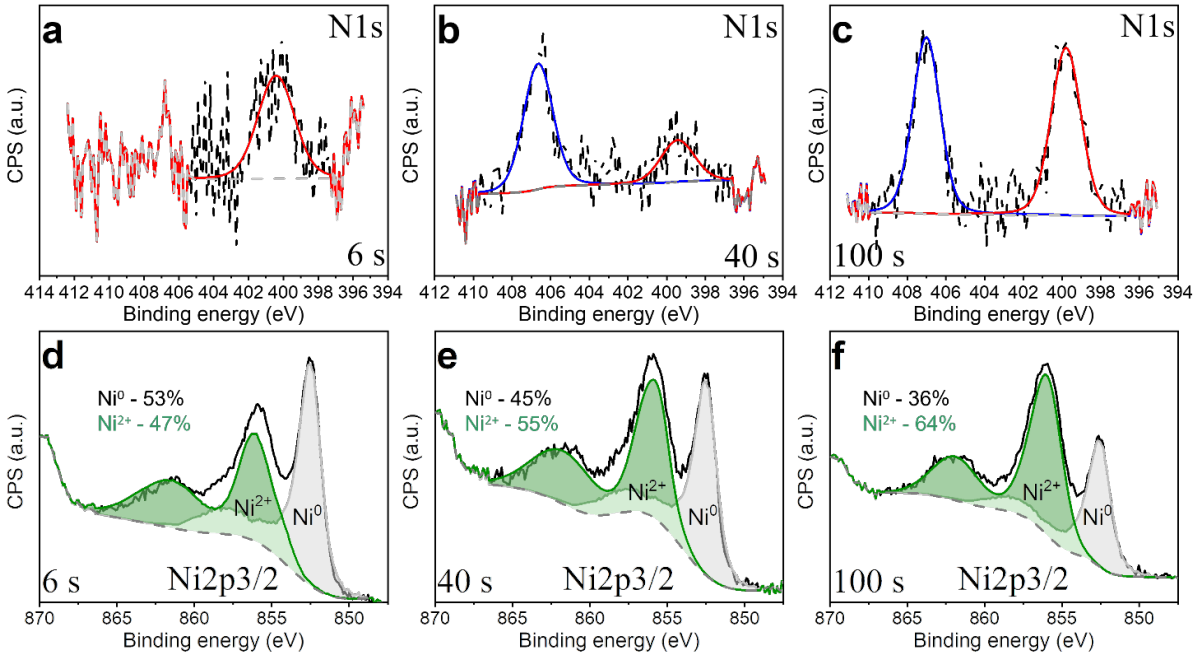

Fig. 6. *Ex situ* N 1s (a, b, c) and Ni $2p_{3/2}$ (d, e, f) XP spectra obtained for polycrystalline Ni after recording OCP in 1 M NaOH + 5mM N_2H_4 for different time: (a, d) 6 s; (b, e) 40 s and (c, f) 100 s.

3.3. Tentative mechanism of the HHOR on Ni electrodes in alkaline media

This section aims to propose a tentative mechanism of the HHOR on Ni in alkaline media, based on the experimental data and analyses presented in sections 3.1 and 3.2; this mechanism is schematically shown in Fig. 7.

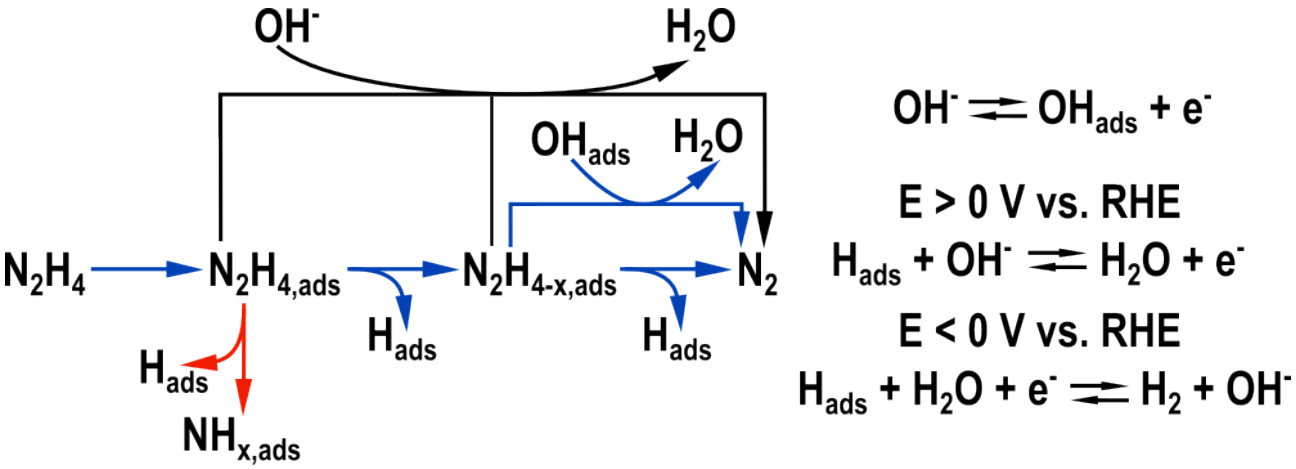

Fig. 7. Tentative HHOR mechanism on metallic Ni electrodes. Black, blue and red lines represent electrochemical, chemical and poisoning steps, respectively.

Considering joint evidence provided by DEMS, electrochemical measurements and *ex situ* XPS, the authors assume that hydrazine, at first, molecularly adsorbs on Ni surface and then decomposes chemically (eq. 10) or electrochemically (eq. 11) forming $N_2H_{4-x,ads}$ intermediates. It must be admitted that distinguishing between the latter steps is hardly possible based on the presented data, and advance in the microkinetic modelling of the HHOR (currently in progress) will surely help.

$$N_2H_{4,ads} \rightleftarrows N_2H_{4-x,ads} + x\ H_{ads} \qquad \text{(eq. 10)}$$

$$N_2H_{4,ads} + x\ OH^- \rightleftarrows N_2H_{4-x,ads} + x\ H_2O + x\ \bar{e}^- \qquad \text{(eq. 11)}$$

The $N_2H_{4-x,ads}$ intermediate can dissociate, further releasing N_2 (eq.12), that is detected with DEMS at potentials where the HHOR currents are not clearly observed yet:

$$N_2H_{4-x,ads} \rightarrow N_2 + (4-x)\ H_{ads} \quad \text{(eq. 12)}$$

Alternatively, evidences provided by this work, notably the "crossing" of the anodic and cathodic scans in CVs (Figs. 2c, 4a, b) and the OCP transient for sample N°1, suggest that the HHOR is strongly enhanced in the presence of OH_{ads}, formed in step 6 at E > 0 V vs. RHE, its surface coverage being larger on the cathodic scan compared to the anodic one (see Fig. 2b). This allows the authors to propose that OH_{ads} either directly reacts with $N_2H_{4-x,ads}$ following step 13 or affects the reactivity of the hydrazine molecule, leading to the complete oxidation (forming N_2) following step 11. Indeed, the DFT calculations show stabilization of more reactive N_2H_4 cis-conformer in the presence of co-adsorbed OH species via electronic interaction [36].

$$N_2H_{4-x,ads} + x\ OH_{ads} \rightleftarrows N_2 + (4-x)\ H_2O \quad \text{(eq. 13)}$$

However, transformation of OH_{ads} into surface α-$Ni(OH)_2$ in step 7 slows down the HHOR, suggesting that α-$Ni(OH)_2$ does not react with hydrazine but rather blocks the surface, hindering hydrazine adsorption into reactive N_2H_{4-x} species.

The adsorbed H_{ads} species, produced in steps 10, 12 can be either ionized (at E > 0 V vs. RHE) following forward step of the equation 5 (Volmer step), or released (at E < 0 V vs. RHE) with the formation of H_2 through the Heyrovsky step 14 of the HER:

$$H_{ads} + H_2O + e^- \rightleftarrows H_2 + OH^- \quad \text{(eq. 14)}$$

The HER competes with the hydrazine adsorption and hence the HHOR at potentials below 0 V vs. RHE.

Finally, along with reactive $N_2H_{4-x,ads}$ intermediates, formation of surface poisons occurs following step 15, likely $NH_{x,ads}$ species:

$N_2H_{4,ads} \rightarrow 2\ NH_{x,ads} + (4-2x)\ H_{ads}$ (poison formation, eq. 15)

This poisoning step depends on the electrode potential, concentration of hydrazine, ECSA, and fraction of other adsorbates on the Ni surface, and is site-demanding, likely requiring larger number of surface sites than steps leading to N_2H_{4-x} formation (eqs. 10, 11).

CONCLUSIONS

Ni nanoparticles as well as polycrystalline Ni were studied in the HHOR by paying special attention to keep Ni surface metallic. Metallic Ni exhibits excellent activity, catalyzing the HHOR from -0.05 V vs. RHE onwards and releasing 4 electrons. No gaseous products except N_2 were detected during the HHOR by DEMS. However, the "onset" potential as well as HHOR currents in the interval from -0.05 and 0.15 V vs. RHE strongly depend on the reaction conditions (ECSA of Ni, hydrazine hydrate concentration) and coverage of Ni surface by other adsorbed species.

Experimental data suggest that hydrazine dissociative adsorption leads to various surface species, notably reactive intermediates (likely $N_2H_{4-x,ads}$) and surface poisons. DEMS data provide evidence for N-H bond dissociation occurring at potential as low as -0.1 V vs. RHE, resulting in a

release of molecular nitrogen and likely H_{ads}, the latter being ionized above 0 V vs. RHE. XPS measurements have shown that most likely the poisoning species are $NH_{x,ads}$; however, further studies are required to reveal their exact nature. The extent of surface poisoning strongly depends on the ECSA of Ni (and hence the number of catalytic sites), hydrazine concentration, and presence of other adsorbates on the Ni surface.

O-containing species on the Ni surface strongly affect hydrazine adsorption and reaction, OH_{ads} being favorable (enhancing the HHOR), while surface α-$Ni(OH)_2$ - unfavorable (blocking the surface and hindering either the HHOR or the surface poisoning).

DECLARATION OF COMPETING INTEREST

The authors declare that they have no known competing financial interests or personal relationships that could have appeared to influence the work reported in this paper.

CREDIT AUTHORSHIP CONTRIBUTION STATEMENT

Evgeniia A. Vorms: Methodology, Investigation, Formal analysis, Writing – original draft, Writing – review & editing. **Vasiliki Papaefthymiou:** Investigation, Writing – review & editing. **Théo Faverge:** Investigation, Writing – review & editing. **Antoine Bonnefont:** Funding acquisition, Supervision, Writing – review & editing. **Marian Chatenet:** Supervision, Writing – review & editing. **Elena R. Savinova:** Funding acquisition, Conceptualization, Supervision, Writing – review & editing. **Alexandr G. Oshchepkov:** Project administration, Conceptualization, Supervision, Writing – original draft, Writing – review & editing.

ACKNOWLEDGMENTS

This work was supported by the Jean-Marie Lehn foundation. The authors express their gratitude to Dr. I. Makarchuk for her assistance with TEM analysis.

SUPPLEMENTARY MATERIALS

Supplementary material associated with this article can be found, in the online version, at doi:

REFERENCES

[1] X. Tian, P. Zhao, W. Sheng, Hydrogen Evolution and Oxidation: Mechanistic Studies and Material Advances, Adv. Mater. 31 (2019). https://doi.org/10.1002/adma.201808066.

[2] L.D. Burke, B.H. Lee, An Investigation of Some Electrocatalytic Processes Occurring at Low Potentials at a Nickel Electrode in Base, J. Electrochem. Soc. 138 (1991) 2496–2504. https://doi.org/10.1149/1.2086008.

[3] T. Sakamoto, K. Asazawa, J. Sanabria-Chinchilla, U. Martinez, B. Halevi, P. Atanassov, P. Strasser, H. Tanaka, Combinatorial discovery of Ni-based binary and ternary catalysts for hydrazine electrooxidation for use in anion exchange membrane fuel cells, J. Power Sources. 247 (2014) 605–611. https://doi.org/10.1016/j.jpowsour.2013.08.107.

[4] S. Zhou, Y. Zhao, R. Shi, Y. Wang, A. Ashok, F. Héraly, T. Zhang, J. Yuan, Vacancy-Rich MXene-Immobilized Ni Single Atoms as a High-Performance Electrocatalyst for the Hydrazine

Oxidation Reaction, Adv. Mater. 34 (2022). https://doi.org/10.1002/adma.202204388.

[5] T.Y. Jeon, M. Watanabe, K. Miyatake, Carbon segregation-induced highly metallic Ni nanoparticles for electrocatalytic oxidation of hydrazine in alkaline media, ACS Appl. Mater. Interfaces. 6 (2014) 18445–18449. https://doi.org/10.1021/am5058635.

[6] J. Zhang, X. Cao, M. Guo, H. Wang, M. Saunders, Y. Xiang, S.P. Jiang, S. Lu, Unique Ni Crystalline Core/Ni Phosphide Amorphous Shell Heterostructured Electrocatalyst for Hydrazine Oxidation Reaction of Fuel Cells, ACS Appl. Mater. Interfaces. 11 (2019) 19048–19055. https://doi.org/10.1021/acsami.9b00878.

[7] Z. Feng, D. Li, L. Wang, Q. Sun, P. Lu, P. Xing, M. An, In situ grown nanosheet Ni Zn alloy on Ni foam for high performance hydrazine electrooxidation, Electrochim. Acta. 304 (2019) 275–281. https://doi.org/10.1016/j.electacta.2019.03.017.

[8] K. Asazawa, K. Yamada, H. Tanaka, M. Taniguchi, K. Oguro, Electrochemical oxidation of hydrazine and its derivatives on the surface of metal electrodes in alkaline media, J. Power Sources. 191 (2009) 362–365. https://doi.org/10.1016/j.jpowsour.2009.02.009.

[9] T. Asset, A. Roy, T. Sakamoto, M. Padilla, I. Matanovic, K. Artyushkova, A. Serov, F. Maillard, M. Chatenet, K. Asazawa, H. Tanaka, P. Atanassov, Highly active and selective nickel molybdenum catalysts for direct hydrazine fuel cell, Electrochim. Acta. 215 (2016) 420–426. https://doi.org/10.1016/j.electacta.2016.08.106.

[10] Y. Lei, Y. Liu, B. Fan, L. Mao, D. Yu, Y. Huang, F. Guo, Facile fabrication of hierarchically porous Ni foam@Ag-Ni catalyst for efficient hydrazine oxidation in alkaline medium, J. Taiwan Inst. Chem. Eng. 105 (2019) 75–84. https://doi.org/10.1016/j.jtice.2019.09.022.

[11] W. Wang, Y. Wang, S. Liu, M. Yahia, Y. Dong, Z. Lei, Carbon-supported phosphatized CuNi nanoparticle catalysts for hydrazine electrooxidation, Int. J. Hydrogen Energy. 44 (2019) 10637–10645. https://doi.org/10.1016/j.ijhydene.2019.03.005.

[12] X. Liu, Y. Li, N. Chen, D. Deng, X. Xing, Y. Wang, Ni3S2@Ni foam 3D electrode prepared via chemical corrosion by sodium sulfide and using in hydrazine electro-oxidation, Electrochim. Acta. 213 (2016) 730–739. https://doi.org/10.1016/j.electacta.2016.08.009.

[13] Q. Qian, J. Zhang, J. Li, Y. Li, X. Jin, Y. Zhu, Y. Liu, Z. Li, A. El-Harairy, C. Xiao, G. Zhang, Y. Xie, Artificial Heterointerfaces Achieve Delicate Reaction Kinetics towards Hydrogen Evolution and Hydrazine Oxidation Catalysis, Angew. Chemie. 133 (2021) 6049–6058. https://doi.org/10.1002/ange.202014362.

[14] Z. Feng, H. Meng, Y. Fu, L. Ren, B. Gao, W. Liu, Modulation of Charge Redistribution in Heterogeneous CoSe-Ni 0.95 Se Coupling with Ti 3 C 2 T x MXene for Hydrazine-Assisted Water Splitting, Small. (2024). https://doi.org/10.1002/smll.202403270.

[15] W. Liu, T. Shi, Z. Feng, Bifunctional zeolitic imidazolate framework-67 coupling with CoNiSe electrocatalyst for efficient hydrazine-assisted water splitting, J. Colloid Interface Sci. 630 (2023) 888–899. https://doi.org/10.1016/j.jcis.2022.10.152.

[16] T. Shi, B. Gao, H. Meng, Y. Fu, D. Kong, P. Ren, H. Fu, Z. Feng, In situ electronic redistribution of NiCoZnP/NF heterostructure via Fe-doping for boosting hydrazine oxidation and hydrogen evolution, Green Chem. 26 (2024) 4209–4220. https://doi.org/10.1039/D4GC00309H.

[17] D.A. Finkelstein, R. Imbeault, S. Garbarino, L. Roué, D. Guay, Trends in catalysis and catalyst cost effectiveness for N2H4 fuel cells and sensors: A rotating disk electrode (RDE) study, J.

Phys. Chem. C. 120 (2016) 4717–4738. https://doi.org/10.1021/acs.jpcc.5b10156.

[18] A.G. Oshchepkov, P.A. Simonov, A.N. Kuznetsov, S.A. Shermukhamedov, R.R. Nazmutdinov, R.I. Kvon, V.I. Zaikovskii, T.Y. Kardash, E.A. Fedorova, O. V. Cherstiouk, A. Bonnefont, E.R. Savinova, Bimetallic NiM/C (M = Cu and Mo) Catalysts for the Hydrogen Oxidation Reaction: Deciphering the Role of Unintentional Surface Oxides in the Activity Enhancement, ACS Catal. 12 (2022) 15341–15351. https://doi.org/10.1021/acscatal.2c03720.

[19] A. Serov, C. Kwak, Direct hydrazine fuel cells: A review, Appl. Catal. B Environ. 98 (2010) 1–9. https://doi.org/10.1016/j.apcatb.2010.05.005.

[20] Y. Ma, H. Li, R. Wang, H. Wang, W. Lv, S. Ji, Ultrathin willow-like CuO nanoflakes as an efficient catalyst for electro-oxidation of hydrazine, J. Power Sources. 289 (2015) 22–25. https://doi.org/10.1016/j.jpowsour.2015.04.151.

[21] L.D. Burke, K.J. O'Dwyer, Mediation of oxidation reactions at noble metal anodes by low levels of in situ generated hydroxy species, Electrochim. Acta. 34 (1989) 1659–1664. https://doi.org/10.1016/0013-4686(89)85044-3.

[22] K. Yamada, K. Yasuda, N. Fujiwara, Z. Siroma, H. Tanaka, Y. Miyazaki, T. Kobayashi, Potential application of anion-exchange membrane for hydrazine fuel cell electrolyte, Electrochem. Commun. 5 (2003) 892–896. https://doi.org/10.1016/j.elecom.2003.08.015.

[23] S.A.S. Machado, L.A. Avaca, The hydrogen evolution reaction on nickel surfaces stabilized by H-absorption, Electrochim. Acta. 39 (1994) 1385–1391. https://doi.org/10.1016/0013-4686(94)E0003-I.

[24] A.G. Oshchepkov, A. Bonnefont, V.A. Saveleva, V. Papaefthimiou, S. Zafeiratos, S.N. Pronkin,

V.N. Parmon, E.R. Savinova, Exploring the influence of the nickel oxide species on the kinetics of hydrogen electrode reactions in alkaline media, Top. Catal. 59 (2016) 1319–1331. https://doi.org/10.1007/s11244-016-0657-0.

[25] A.G. Oshchepkov, A. Bonnefont, E.R. Savinova, On the influence of the extent of oxidation on the kinetics of the hydrogen electrode reactions on polycrystalline nickel, Electrocatalysis. 11 (2020) 133–142. https://doi.org/10.1007/s12678-019-00560-3.

[26] A.G. Oshchepkov, A. Bonnefont, V.N. Parmon, E.R. Savinova, On the effect of temperature and surface oxidation on the kinetics of hydrogen electrode reactions on nickel in alkaline media, Electrochim. Acta. 269 (2018) 111–118. https://doi.org/10.1016/j.electacta.2018.02.106.

[27] E. Santos, P. Hindelang, P. Quaino, E.N. Schulz, G. Soldano, W. Schmickler, Hydrogen electrocatalysis on single crystals and on nanostructured electrodes, ChemPhysChem. 12 (2011) 2274–2279. https://doi.org/10.1002/cphc.201100309.

[28] A.G. Oshchepkov, G. Braesch, A. Bonnefont, E.R. Savinova, M. Chatenet, Recent Advances in the Understanding of Nickel-Based Catalysts for the Oxidation of Hydrogen-Containing Fuels in Alkaline Media, ACS Catal. 10 (2020) 7043–7068. https://doi.org/10.1021/acscatal.0c00101.

[29] A. Zadick, J.F. Petit, V. Martin, L. Dubau, U.B. Demirci, C. Geantet, M. Chatenet, Ubiquitous Borane Fuel Electrooxidation on Pd/C and Pt/C Electrocatalysts: Toward Promising Direct Hydrazine-Borane Fuel Cells, ACS Catal. 8 (2018) 3150–3163. https://doi.org/10.1021/acscatal.7b04321.

[30] P.M. Sipos, G. Hefter, P.M. May, Viscosities and Densities of Highly Concentrated Aqueous MOH Solutions (M + = Na + , K + , Li + , Cs + , (CH 3) 4 N +) at 25.0 °C, J. Chem. Eng. Data. 45 (2000) 613–617. https://doi.org/10.1021/je000019h.

[31] E. Laksono, A. Galtayries, C. Argile, P. Marcus, Adsorption of NH3 on oxygen pre-treated Ni(111), Surf. Sci. 530 (2003) 37–54. https://doi.org/10.1016/S0039-6028(03)00267-X.

[32] D.J. Alberas, J. Kiss, Z.-M. Liu, J.M. White, Surface chemistry of hydrazine on Pt(111), Surf. Sci. 278 (1992) 51–61. https://doi.org/10.1016/0039-6028(92)90583-R.

[33] A. Galtayries, E. Laksono, J.-M. Siffre, C. Argile, P. Marcus, XPS study of the adsorption of NH3 on nickel oxide on Ni(111), Surf. Interface Anal. 30 (2000) 140–144. https://doi.org/10.1002/1096-9918(200008)30:1<140::AID-SIA820>3.0.CO;2-5.

[34] W. Ranke, UPS and XPS reference data of O, N, NO, (NO2)2, NH3, H2O, OH, H2S, SH and S on Ge surfaces, J. Electron Spectros. Relat. Phenomena. 61 (1993) 231–240. https://doi.org/10.1016/0368-2048(93)80053-O.

[35] J. Baltrusaitis, P.M. Jayaweera, V.H. Grassian, XPS study of nitrogen dioxide adsorption on metal oxide particle surfaces under different environmental conditions, Phys. Chem. Chem. Phys. 11 (2009) 8295. https://doi.org/10.1039/b907584d.

[36] M.K. Agusta, P.H. Purwoko, A.G. Saputro, F. Fathurrahman, H.K. Dipojono, W.A. Diño, Conformational effects on hydrazine and OH coadsorption on Ni(111): A first-principles investigation, Surf. Sci. 664 (2017) 185–193. https://doi.org/10.1016/j.susc.2017.06.013.